RSC Advances

PAPER

View Article Online
View Journal | View Issue

Cite this: *RSC Adv.*, 2023, **13**, 24174

Experimental determination and thermodynamic optimization of the LiF-NdF_3 system

ChunFa Liao,[ab] ZanHui Fu,[ab] LiangHua Que,[ab] Hao Tang[ab] and Xu Wang*[ab]

Received 6th May 2023
Accepted 7th August 2023

DOI: 10.1039/d3ra03003b

rsc.li/rsc-advances

Neodymium is mainly obtained by electrolysis of a molten LiF-NdF_3-Nd_2O_3 system. LiF-NdF_3 is a basic system, and the phase diagram of this system provides important information in the production of electrolytic neodymium. An accurate LiF-NdF_3 binary phase diagram helps in the selection of the appropriate molten salt component in production and optimizing the production process, which is of great significance to improve the electrolysis efficiency and reduce the production cost. To obtain an accurate phase diagram of the LiF-NdF_3 binary system, liquidus and solidus temperatures were experimentally determined in the LiF-NdF_3 binary system by differential scanning calorimetry. The experimental results were used to construct the phase diagram and develop a new database for the LiF-NdF_3 system using the FactSage software. The sub-regular solution model was used to describe the excess Gibbs free energy of the liquid phase, and the thermodynamic optimization calculation was carried out for the binary system. The binary interaction coefficients ${}^0L = -39\,966 + 17.68\,T$, ${}^1L = -7667 + 26.1\,T$, and ${}^2L = -6000$ were used to describe the system's excess Gibbs free energy. The results show that the eutectic point of the system is 68.4% LiF-31.6% NdF_3 at 731.5 °C. The effects of industrial and high purity NdF_3 and the presence of Nd_2O_3 on the liquidus temperature of the LiF-NdF_3 system were also investigated, high liquidus temperatures have been observed in tests using industrial NdF_3 and NdF_3 feedstock that contains a specific quantity of Nd_2O_3.

1. Introduction

Neodymium is a metal that is widely used in the field of key rare-earth functional materials, such as NdFeB magnetic materials, rare-earth alloys, and rare-earth hydrogen-storage materials.[1,2] The main preparation method is molten salt electrolysis, and the electrolytic system mainly includes chloride and fluoride salt systems. The fluorine salt system is currently used for industrial production. In the molten salt electrolysis process, rare-earth fluoride is the electrolyte, and rare-earth oxide is electrolytic raw material. Currently, REF_3-LiF and REF_3-LiF-BaF_2 electrolyte systems are commonly used.[3,4] The solubility and eutectic temperature of rare-earth oxides in the REF_3-LiF molten salt system are the key factors affecting electrolytic neodymium's production process.[5] Research into phase diagrams can provide many useful pieces of information for developing new materials: Fedrov *et al.*[6] reviewed lithium rare-earth fluorides as photonic materials, citing many phase diagrams that can provide theoretical guidance for optimizing production processes. The construction methods of phase diagrams mainly include the experimental determination method[7] and the CALPHAD phase diagram calculation method.[8,9] A large amount of experimental data is required to determine phase diagrams, and the accuracy of the phase diagram is greatly affected by the purity of the raw materials, as well as the accuracy of the analysis and experimental operation, which means that it has the disadvantages of a large workload and requires a high level of manpower, large quantities of materials, and substantial financial resources. Phase diagrams are difficult to determine through experiments only, and thermodynamic calculations of phase diagrams are often limited by a lack of accurate thermodynamic data. Experimental and thermodynamic data on the LiF-NdF_3 system's binary phase diagrams are lacking, with Thoma data and Xue data among the few experimental data found so far. Marcelle Gaune-Escard *et al.*[10] analyzed the enthalpy of mixing NdF_3-MF (M = Li, Na, K) binary systems data using the Hoch–Arpshofen solution model, and with the development of CALPHAD phase diagram calculation technology, the construction of phase diagrams by combining experimental determination with phase diagram calculation has been widely adopted by scientific and technological workers.[11,12]

Thoma *et al.*[13] studied the phase diagram of LiF-NdF_3 by thermal analysis experiments; however, the raw NdF_3 material used in the experiments was prepared from the transformation of rare-earth oxide, which had a high level of rare-earth oxide (300 ppm). Nd_2O_3 in the raw material had considerable

[a]*Faculty of Materials Metallurgy and Chemistry, Jiangxi University of Science and Technology, Ganzhou 341000, China. E-mail: sci_rech@163.com*

[b]*National Rare Earth Functional Materials Innovation Center, Ganzhou 341000, China*

influence on the measurement result of liquidus temperatures. In terms of phase diagram calculation, Van der Meer *et al.*[14] calculated the NdF_3-LiF binary phase diagram by using the CALPHAD method and ChemSage software. They used the Redlich–Kister polynomial to describe the excess free energy of the liquid phase based on the literature experimental data.[13] The calculated phase diagram is consistent with the experimental phase diagram in literature.[13] M. Berkani *et al.*[15] calculated the LiF-NdF_3 binary phase diagram by thermal analysis and the Hoch–Arpshofen model. A. Abbasalizadeh *et al.*[16] conducted experimental research and thermodynamic modeling on the LiF-NdF_3-DyF_3 ternary system, as well as Gibbs free energy modeling of the LiF-NdF_3 and LiF-DyF_3 systems by using the literature data.[13] The phase diagram of the LiF-NdF_3 binary system was calculated by the CALPHAD method. Xue *et al.* used DTA analysis to measure the liquidus temperature of the NdF_3-LiF binary system at various compositions,[17] drew the experimental phase diagram according to the results of the DTA, and finally optimized the LiF-NdF_3 binary phase diagram according to CALPHAD calculation; however, the experimental materials used were all industrial grade with impurities. The peak temperature of the DTA curve was considered the result of liquidus temperature, and the optimized phase diagram of the LiF-NdF_3 binary system obtained by this method still requires further discussion. Johnathon C. Ard *et al.*[18] assessed and then reassessed the thermodynamics of 30 pseudo-binary and ternary salt systems, assessed the LiF-NdF_3 binary phase diagram by modified quasi-chemical model in the quadruplet approximation with the data from literature,[13] and determined relations for the liquid interaction parameters, and the phase diagram was in good agreement with literature.[13] Regarding for the bivariate phase diagram of LiF-NdF_3 that was previously described, the experimental method measured the phase diagrams,[13,17] however, the raw material used in the ref. 17 experiment is industrial level, and its phase diagram is only suitable for guiding production. The other is a phase diagram that was calculated using experimental data found in literature.[13] Additionally, the experimental NdF_3 material utilized in ref. 13 is not high pure, which will significantly affect the experiment's results. For the purpose of obtaining more accurate phase diagram and thermodynamic data, this research combines the phase diagram calculation technique with higher purity raw materials to measure the solidus and liquidus temperature. Thermodynamic data consistent with the phase diagram can provide basic data for the study of the LiF-NdF_3-Nd_2O_3 ternary phase diagram, which has important practical significance and economic value for optimizing the rare earth neodymium production process, improving current efficiency and reducing production costs. Therefore, differential scanning calorimetry was used to investigate the liquidus and solidus temperatures of the LiF-NdF_3 system with different components. FactSage software was employed to calculate and optimize the phase diagram of the LiF-NdF_3 molten salt system. The thermodynamic parameters of the system were optimized, and an accurate LiF-NdF_3 phase diagram was constructed by combining the experiment with the CALPHAD method.

2. Experimental methods

2.1. Thermal analysis experiment

Raw materials for thermal analysis experiment: LiF, NdF_3 and $Nd_2O_3$with purity ≥ 99.99% were obtained from Shanghai Macklin Biochemical Technology Co., Ltd. Industrial grade NdF_3 obtained from Nanjing Chemical Reagent Co., Ltd.

2.1.1. Instrument. Differential scanning calorimeter (model STA449 F5) was made by Germany NETZSCH Instrument Manufacturing Co., Ltd.

2.1.2. Sample preparation. LiF and NdF_3 were dried at 150 °C for 24 hours prior to preparation to remove possible moisture in the reagent. LiF-NdF_3 mixtures of different mass ratios were prepared and ground repeatedly in an agate mortar for half an hour so that LiF and NdF_3 could be thoroughly mixed, and the preparation process was carried out in a glove box filled with nitrogen gas.

2.1.3. Experiment condition. Thermal analysis experiments were carried out in a nitrogen atmosphere using a platinum crucible. The nitrogen flow velocity was 20 ml min^{-1}, the sample weight was 10–20 mg, the highest test temperature was 1000 °C, the lowest test temperature was 600 °C, and the heating and cooling rates were 10 °C min^{-1}. The experimental temperature control program is shown in Fig. 1.

2.2. Phase diagram calculation

Based on the experimental phase diagram, the Gibbs freedom of the LiF-NdF_3 system was calculated and optimized using the compound, solution, equilib, optisage, and phase diagram module of FactSage8.1 software. A new compound database and liquid phase database were created in the compound and solution modules, respectively. The interaction coefficient ${}^{i}L$ was optimized by the Bayesian optimization algorithm based on the probability model and constantly adjusted until the optimized phase diagram was in good agreement with the experimental phase diagram.[19] The optimized thermodynamic data and optimized phase diagram of the system were obtained.

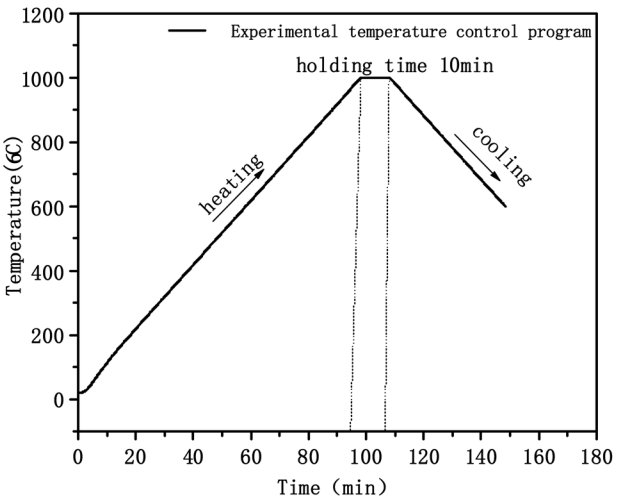

Fig. 1 Experimental temperature control procedure.

3. Results and discussion

3.1. Experimental results and discussion of thermal analysis

3.1.1. Experimental principle of thermal analysis. The sample exhibited evident endothermic or exothermic phenomena during the phase transformation in the heating and cooling processes. The initial temperature of the endothermic peak is extrapolated from the heating DSC curve as the solidus temperature, and the temperature of the intersection between the tangent line of the maximum slope of the first exothermic peak of the cooling DSC curve and the baseline is considered the liquidus temperature.[5,20] The reason we obtain the solidus and liquidus temperatures from the different DSC curves is that we observed that the cooling curve is prone to deviation when determining the solidus temperature, which may result in a larger error when the experimental temperature is higher; therefore, we recommend using the heating and cooling curves to determine the solidus and liquidus temperatures, respectively.[21] Fig. 2(a) and (b) show the DSC heating and cooling curves of the binary system LiF-1% NdF_3, respectively, according to the method. The LiF-NdF_3 system's liquidus and solidus temperatures are 846.5 °C and 728.4 °C, respectively. Similarly, the liquidus and solidus temperatures of other component samples can be determined.

3.1.2. Experimental results of thermal analysis. Reports indicate that the melting temperature of LiF is 847.5 °C,[22,23] while that of NdF_3 is 1374 °C,[22] however, some reports show that the melting temperature of NdF_3 is 1413 °C.[23] Therefore, the melting temperature of pure-substance LiF was measured with a calibrated thermal analyzer, and the tangent method was used to analyze the DSC heating curve of LiF.[24] Fig. 3 shows that the measurement result is 847.6 °C. The melting temperature of LiF is determined at 847.5 °C, considering the influence of experimental errors. At the same time, the reliability of analyzing the solidus temperature of the molten salt system by the DSC heating curve with tangent method is verified. The melting temperature of NdF_3 at 1374 °C,[22] which was reported in the same literature as LiF, was adopted.

Table 1 shows the liquidus and solidus temperatures of the LiF-NdF_3 molten salt system with different mass fractions tested experimentally. In accordance with the liquidus and solidus temperatures of the LiF-NdF_3 system measured by thermal analysis, the experimental results show that, when the molar concentration of NdF_3 is less than 31%, as the mole fraction of NdF_3 in the system increases, the liquidus temperature of the LiF-NdF_3 molten salt system gradually decreases. In addition, when the molar concentration of NdF_3 is greater than 31%, as the increase in the mole fraction of NdF_3 in the system increases, the liquidus temperature of the LiF-NdF_3 system gradually increases. This finding shows that LiF can significantly reduce the liquidus temperature of the molten salt system, and with the increase in the mole fraction of NdF_3, the liquidus temperature of the LiF-NdF_3 system gradually increases mainly due to the high melting temperature of NdF_3. The samples of different components have the same solidus temperature, which also indicates that the LiF-NdF_3 system is

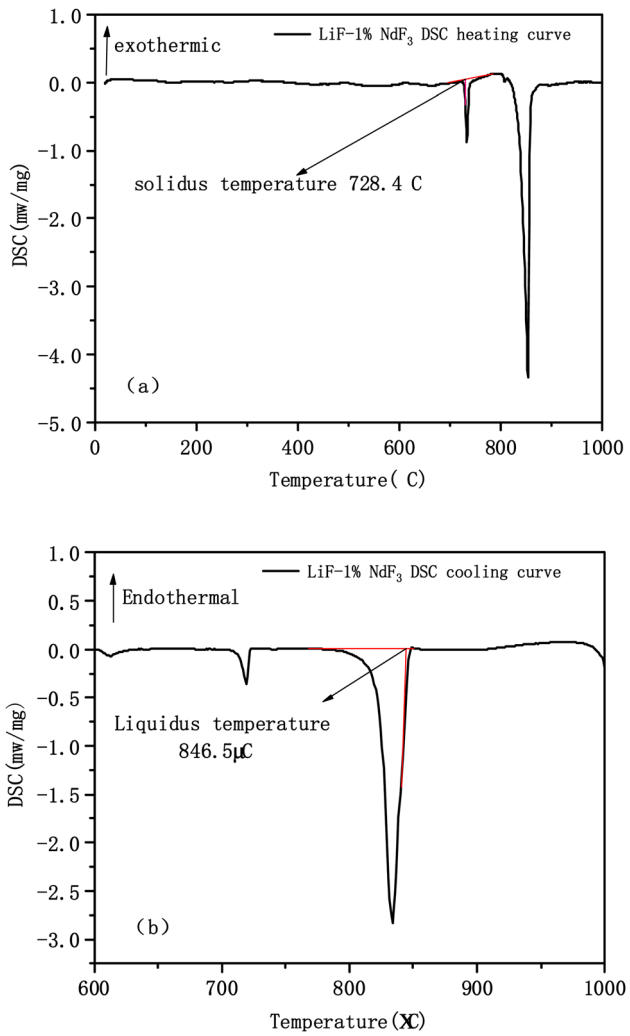

Fig. 2 Schematic of solidus and liquidus temperatures analysed by DSC curve: (a) LiF-1% NdF_3 DSC heating curve; (b) LiF-1% NdF_3 DSC cooling curve.

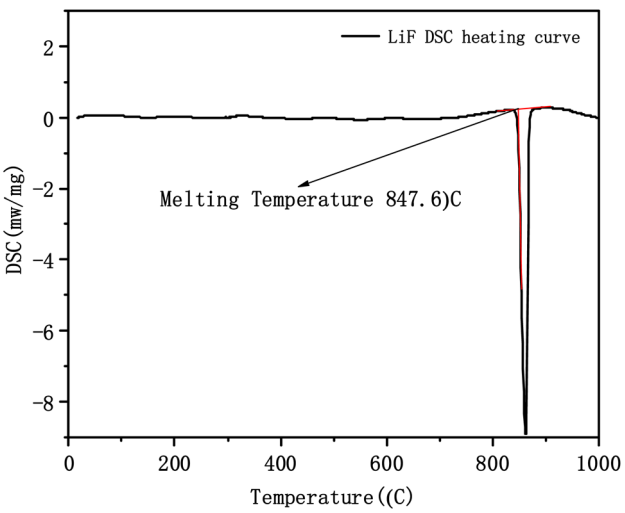

Fig. 3 LiF DSC heating curve.

Table 1 DSC curve analysis results of different compositions of LiF-NdF_3 system

No.	LiF mol%	NdF_3 mol%	Liquidus temperature (°C)	Solidus temperature (°C)	Ref.
1	100	0	847.5		22
2	99	1	846.5	728.4	
3	97	3	841.1	728.3	
4	95	5	832.6	727.1	
5	92	8	832.7	728.8	
6	90	10	821.8	726.1	
7	89	11	798.3	729.2	
8	84	16	793.6	728.2	
9	81	19	788.8	729.3	
10	77	23	776.9	729.7	
11	72	28	752.2	728.3	
12	69	31	734.6	729.1	
13	67	33	745.4	729.4	
14	66	34	751.1	728.4	
15	63	37	782.0	730.6	
16	60	40	790.5	724.4	
15	0	100	1374		22

a low eutectic system without the formation of intermediate compounds, which is consistent with the results of previous studies.

Table 2 shows the regression equation, indicating that the intersection of the two fitted lines is the eutectic point of the LiF-NdF_3 system. After calculation, the eutectic temperature of the system is 736.6 °C, and the eutectic components are divided into 68.62% LiF-31.38% NdF_3.

3.2. LiF-NdF_3 phase diagram calculation and thermodynamic optimization

3.2.1. Theoretical basis of phase diagram calculation. The first step to describe the phases of the LiF-NdF_3 molten salt system is to define the Gibbs free energy functions for all the compounds and mixtures in the system. In most instances, the excess Gibbs free energy function is unknown. Therefore, thermodynamic evaluation is required to determine the excess Gibbs free energy. The Gibbs free energy equation of the compound is a function of enthalpy and entropy at the standard temperature state (298.15 K), as follows:

$$G(T) = H(T) - S(T)T \quad (1)$$

$$H(T) = H^0_{298.15} + \int_{298.15}^{T} C_p \mathrm{d}T \quad (2)$$

$$S(T) = \int_0^T \frac{C_p}{T} \mathrm{d}T \quad (3)$$

C_p function can be obtained by the fitting group experimental data:

$$C_p = a + bT + cT^{-2} \quad (4)$$

In the LiF-NdF_3 binary molten salt system, the pure components are LiF and NdF_3, the crystal structures are shown in Table 3, and the Gibbs free energy for pure components can be expressed as a function of temperature, as follows:

$$G(T) = \Delta H^0_{298.15\ \mathrm{K}} - T\Delta S^0_{298.15\ \mathrm{K}} + \int_{298.15\ \mathrm{K}}^{T} C_p \mathrm{d}T - T \times \int_{298.15\ \mathrm{K}}^{T} \frac{C_p}{T} \mathrm{d}T = a + bT + cT \ln T + \mathrm{d}T^2 + eT^{-1} \quad (5)$$

where $\Delta H298.150$ and $\Delta S298.150$ are the standard enthalpy and standard entropy of the standard state (1 bar) at 298.15 K, respectively; C_p is the isobaric heat capacity of each pure substance; a, b, c, d, and e are the parameters to be determined; and T is the thermodynamic absolute temperature, K. Specific data are shown in Table 4, and the related thermodynamic parameters of pure components are obtained from the FactSage database.[25]

The most commonly used thermodynamic models for phase diagram calculation are the ideal solution, regular solution, compound energy, modified association models, as well as the modified quasi-chemical model in the quadruplet

Table 2 Regression equation of liquidus temperature (°C) for LiF-NdF_3 binary system[a]

Range (mol%)	Fitted equation
$x_{NdF_3} > 31\%$	$Y = 577.59 + 374.2858 \times C + 422.1014 \times C^2$
$x_{NdF_3} \leq 31\%$	$Y = 848.59 - 287.4729 \times C - 220.8428 \times C^2$

[a] Note: Y—liquidus temperature (°C); C—mole fraction of NdF_3.

Table 3 Phase and crystal structure adopted for thermodynamic calculation of the LiF-NdF_3 system

Phase	Space groups	Crystal structure	Descriptive model
Liquid	—	—	[LiF, NdF_3]
LiF	*Fm3m*	Cubic	LiF
NdF_3	*P6c2*	Hexagonal	NdF_3

Table 4 Thermodynamic parameters of LiF and NdF_3 pure substances

Phase	$\Delta H_{298.15}$ kJ mol^{-1}	$S_{298.15}$ J mol^{-1} K^{-1}	Temperature, K	C_p J mol^{-1} K^{-1}
LiF (solid)	−616.931	35.65	298.15–1121.3	$C_p = 42.69 + 14.41 \times 10^{-3}\,T - 5.30 \times 10^5 \times T^{-2}$
LiF (liquid)	−594.58	43.00	1121.3–1900	64.183
NdF_3 (solid)	−1679.458	120.792	298.15–1650	$C_p = 92.697 + 23.43 \times 10^{-3} \times T - 6.456 \times 10^5 \times T^{-2}$
NdF_3 (liquid)	−1607.88	340.77	1650–1800	$C_p = 184.473 - 4.435 \times 10^{-3}\,T - 119.244 \times 10^5 \times T^{-2}$

approximation.[26] The regular solution model[27] was proposed by Hildebrand in 1929, assuming the actual melt to be a replacement melt, and it is well simulated in some simple melt systems. The LiF-LuF_3 molten salt systems (Lu = La, Ce, Pr, Nd, Sm, U and Pu) are all phase diagram systems with a low eutectic point without forming an intermediate, therefore, the thermodynamic LiF-NdF_3 molten salt system can be described by the sub-regular solution model. Moreover, in the literature,[15–17] the regular solution model was used to calculate the phase diagram of the LiF-NdF_3 binary system.

For the liquid phase of the LiF-NdF_3 binary system, the sub-regular solution model was used to describe the Gibbs free energy in the liquid phase. The Gibbs free energy is composed of pure-component mechanical mixing to Gibbs free energy, an ideal mixing contribution to Gibbs free energy, and excess Gibbs free energy.[28–30] The expression is as follows:

$$G^{\text{liquid}} = {}^{\text{ref}}G_{\text{m}}^{\text{liquid}} + {}^{\text{id}}G_{\text{m}}^{\text{liquid}} + {}^{\text{ex}}G_{\text{m}}^{\text{liquid}} \quad (6)$$

$${}^{\text{ref}}G_{\text{m}}^{\text{liquid}} = \sum x_i\,{}^{0}G_{\text{m}}^{\text{liquid}} \quad (7)$$

$${}^{\text{id}}G_{\text{m}}^{\text{liquid}} = RT\sum x_i \ln(x_i) \quad (8)$$

where ${}^{\text{ref}}G_{\text{m}}{}^{\text{liquid}}$ is the contribution of pure-component mechanical mixing to Gibbs free energy, ${}^{\text{id}}G_{\text{m}}{}^{\text{liquid}}$ is the contribution of ideal mixing entropy to Gibbs free energy, and ${}^{\text{ex}}G_{\text{m}}{}^{\text{liquid}}$ is the part of the non-ideal mixture, that is, the contribution of the excess Gibbs free energy. The excess Gibbs free energy was expressed by the Redlich–Kister polynomial.[31] When calculating the LiF-NdF_3 binary phase diagram, the thermodynamic model can be described as follows:

$${}^{ex}G^{\text{liquid}}_{\text{Li}^+,\text{Nd}^{3+}:\text{F}^-} = x_{\text{LiF}}x_{\text{NdF}_3}\sum_{i=0}^{n} {}^{i}L^{\text{liquid}}_{\text{Li}^+,\text{Nd}^{3+}:\text{F}^-}\left(x_{\text{Li}^+} - x_{\text{Nd}^{3+}}\right)^i \quad (9)$$

where the parameter ${}^{i}L$ has a linear relationship with temperature and can be described as follows:

$${}^{i}L = a + bT \quad (10)$$

where x_{LiF} and x_{NdF_3} are the mole fractions of LiF and NdF_3, respectively, and ${}^{i}L$ is the binary interaction coefficient of order i. When $i = 0$, ${}^{\text{ex}}G_{\text{m}}{}^{\text{liquid}}$ becomes a regular solution model, and when $i = 1$, ${}^{\text{ex}}G_{\text{m}}{}^{\text{liquid}}$ becomes a sub-regular solution model. In general, the value of i is not greater than 2, and a and b are parameters that should be optimized.

3.2.2. Phase diagram calculation and thermodynamic optimization. Table 5 shows the optimized system thermodynamic data and thermodynamic interaction parameters, while Fig. 4 shows the optimized phase diagram, both according to the phase diagram calculation method described in Section 2.2.

Under the system's optimized thermodynamic data, the liquidus temperatures of each experimental component were

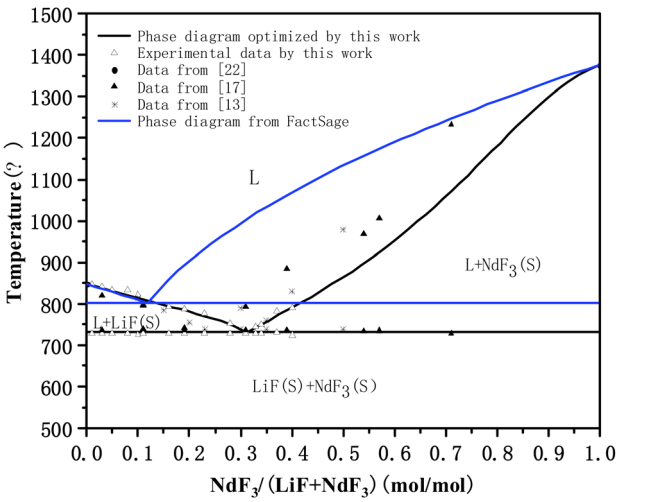

Fig. 4 Comparison between optimized LiF-NdF_3 binary phase diagram and experimental data. * The blue line was calculated directly by FactSage software, which was not optimized.

Table 5 Thermodynamic optimization parameters of LiF-NdF_3 binary molten salt system

System	Phase	Gibbs free energy parameter (J mol^{-1})
LiF-NdF_3	LiF	S: $G = -628\,236.010 + 258.443\,T - 42.689T\ln T - 0.009\,T^2 + 265\,056.4\,T^{-1}$ (298.15–1121.3 K)
		L: $G = -613\,717.638 + 386.871\,T - 64.183T\ln T$ (1121.3–2000 K)
	NdF_3	S: $G = -1\,686\,591.566 + 386.191\,T - 74.977T\ln T - 0.0183\,T^2 - 1\,014\,620\,T^{-1}$ (298.15–1650 K)
		L: $G = -1\,765\,032.569 + 1208.505\,T - 184.473T\ln T + 0.002\,T^2 + 5\,962\,200\,T^{-1}$ (1650 − 1900 K)
		${}^{0}L^{\text{liquid}}_{\text{Li}^+,\text{Nd}^{3+}:\text{F}^-} = -39\,966 + 17.68\,T$
		${}^{1}L^{\text{liquid}}_{\text{Li}^+,\text{Nd}^{3+}:\text{F}^-} = -7667 + 26.1\,T$
		${}^{2}L^{\text{liquid}}_{\text{Li}^+,\text{Nd}^{3+}:\text{F}^-} = -6000$

Table 6 Experimental results comparing high purity and industrial NdF_3

No.	Component	Liquidus temperature with high purity NdF_3 (°C)	Liquidus temperature with industrial NdF_3 (°C)
1	LiF-23% mol NdF_3	776.9	805.0
2	LiF-31% mol NdF_3	734.6	802.4
3	LiF-37% mol NdF_3	782.0	797.6
4	LiF-40% mol NdF_3	790.5	798.2

calculated using the Equilib module in FactSage, with the maximum, minimum, and average deviations being 12.54 °C, −0.53 °C, and 3.28 °C, respectively. The eutectic temperature of the optimized phase diagram is 731.5 °C, and the eutectic point of the system is 68.4% LiF-31.6% NdF_3. The result is very close to the intersection of the two fitted lines calculated in Section 3.1.2, showing that the calculated phase diagram is in good agreement with the experimental phase diagram. Moreover, describing the Gibbs free energy of the LiF-NdF_3 molten salt system is feasible by using the sub-regular solution model. The calculated phase diagram is accurate and reliable.

Fig. 4 shows that the phase diagram obtained in this work (calculated directly by FactSage software (the blue line)) and the phase diagrams in the ref. 13 and 17 are all simple binary phase diagrams formed without intermediates. The liquidus trend is the same, but there are some differences. The eutectic point position and liquidus temperature at the low LiF side of the system are different. We also noticed that the obtained phase diagram was different from the literature,[17] although the trend in the temperature of the liquids is consistent, and the composition of eutectics in this paper is 68.4% LiF-31.6% NdF_3 and 77% LiF-23% NdF_3 in literature.[17] The difference might be caused by the equipment being tested, the purity of the raw materials, or other factors. At the same time, the final result may be slightly different because the phase diagram is optimized by different thermodynamic models. The phase diagram that calculated by FactSage directly is the phase diagram without thermodynamic evaluation and optimization, meaning it does not consider the influence of excess Gibbs free energy on the system. However, there is possibility of improvement in the FactSage LiF-NdF_3 binary system database through the optimized thermodynamic data from the literature.

As is well known that NdF_3 is primarily based on Nd_2O_3 as a raw material for fluorine conversion preparation, that its conversion rate is affected by the production process, that different production processes or requirements for purity are different, that its conversion rate will be different, and that for raw materials of industrial grade, it is typically believed that NdF_3 purity must be greater than 99.0% to satisfy the requirements. To learn more about how various NdF_3 raw materials affect the liquidus temperature of the LiF-NdF_3 binary phase diagram, four comparison experiments were conducted using high-purity NdF_3 (purity ≥ 99.99%) and industrial NdF_3 (purity ≥ 99.0%) as the raw materials. Because the liquidus temperature of LiF-NdF_3 obtained in this paper on the side with high NdF_3 content is significantly lower than the data obtained in the literature.[17] Table 6 displays the findings of the DSC test. According to the results of the experiments, when NdF_3 is tested with industrial purity, the liquidus temperature is clearly higher than when NdF_3 is tested with high purity raw material under the same conditions. The experiments show that when NdF_3 is tested with industrial purity, for example, the industrial raw material tested this time had a liquidus temperature of 802.4 °C, which is almost identical to the 793.6 °C found in the literature[17] for the LiF-31% mol NdF_3 component. This discrepancy may be caused by the different raw material sources, though. The temperature of 734.6 °C that was tested using raw materials of high purity is substantially lower than both of the results.

Simultaneously, to demonstrate the influence of Nd_2O_3 impurities on the liquidus temperature of the LiF-NdF_3 binary phase diagram, the liquidus temperature of the LiF-23% mol NdF_3 system was 793.8 °C, 781.1 °C, and 803.0 °C after adding the mass fractions of Nd_2O_3 of 0.5%, 1.0%, and 2.0%, respectively. The experimental results demonstrate that, in comparison to the system without Nd_2O_3, the liquidus temperature of the LiF-NdF_3 system rises with varied mass fractions of Nd_2O_3.

To sum up, on the low NdF_3 side, the experimental data and optimized liquidus temperature in this work are basically consistent with those in ref. 13 and 17; however, on the low LiF side, the experimental data and optimized liquidus temperature obtained in this work are significantly lower than those in ref. 13 and 17, which may be related to the purity of the NdF_3 used in the experiments mentioned above, because higher levels of Nd_2O_3 or other impurities will affect the liquidus temperature of the system and cause the eutectic point position to shift to the lower NdF_3 position. This can also explain why the phase diagram in our work is basically consistent with the phase diagram in the literature on the low NdF_3 side, while there is a larger difference on the low LiF side.

4. Conclusions

The thermal properties of the LiF-NdF_3 binary molten salt system were examined in this study using differential scanning calorimetry. The results acquired from this analysis were utilized a relationship between the component's melting temperature and its NdF_3 content. When $x_{NdF3} > 31\%$, $Y = 577.59 + 374.2858 \times C + 422.1014 \times C^2$, and when $x_{NdF_3} \leq 31\%$, $Y = 577.59 + 374.2858 \times C + 422.1014 \times C^2$. In LiF-$NdF_3$-$Nd_2O_3$ molten salt systems, the regression equation can be used as a guide for altering and optimizing the rare-earth neodymium electrolysis process.

The LiF-NdF_3 binary system's liquidus temperature test findings are significantly influenced by the purity of NdF_3, and

they are likely to deviate greatly if Nd_2O_3 or other impurities are present in the raw material. As a result, the experimental phase diagram of the LiF-NdF_3 binary system was chosen for this paper with a purity of at least 99.99% and is reliable.

The thermodynamic parameters of the basic molten salt LiF-NdF_3 binary system for the electrolysis of molten salt fluoride and neodymium oxide were optimized using the CALPHAD phase diagram calculation technology, FactSage software, and sub-regular solution model. The thermodynamic data of the LiF-NdF_3 system were improved, and an accurate LiF-NdF_3 binary phase diagram was constructed in combination with the experimental data, providing basic data for the construction of the LiF-NdF_3-Nd_2O_3 ternary phase diagram in the next procedure.

More studies are needed on the binary phase diagram of LiF-NdF_3 that obtained by experimental and CALPHAD methods because the simulation of the system is a very complicated project. In future research, it is necessary to obtain additional experimental data and select more accurate thermodynamic models to optimize phase diagram simulations by comparing the optimization effects of different thermodynamic models. For example, the ref. 18 optimized the phase diagram of LiF-NdF_3 binary systems by using the modified quasi-chemical model in quadruplet approximation. More thermodynamic data were needed to research the LiF-NdF_3 binary system. When the experimental data is sufficient, the thermodynamic data is complete and the optimization is more reasonable, the phase diagram of LiF-NdF_3 will become more and more accurate.

Conflicts of interest

There are no conflicts to declare.

Acknowledgements

This work was supported by the National Natural Science Foundation of China (grant numbers 52174335, 52074134).

Notes and references

1 H. C. Lin, *Rare Earth*, 2002, **23**(2), 73–77.
2 L. Q. Ji, M. X. Chen, H. Gu, J. H. Zhao and X. Yang, *Chin. J. Rare Earth*, 2020, **38**(2), 129–138.
3 W. Y. Wu and J. S. Zhang, *Non-ferrous mining and metallurgy*, 2000, **16**(6), 34–36.
4 Y. J. Liu and S. H. Yan, *Rare Earth*, 2003, **4**, 2–8.
5 C. F. Liao, S. M. Chen, X. Wang, B. Q. Cai, J. Y. Lin, Y. F. Jiao and Y. L. Zeng, *J. Rare Earths*, 2019, **37**(2), 211–217.
6 P. P. Fedorov, V. V. Semashko and S. L. Korableva, *Inorg. Mater.*, 2022, **58**(3), 223–245.
7 L. Chi, MS thesis, Shanghai University, 2004.
8 Y. W. Li, K. K. Chang, P. S. Wang, B. Hu, L. J. Zhang, S. H. Liu and Y. Du, *Mater. Sci. Eng. Powder Metall.*, 2012, **17**(1), 1–9.
9 Q. Luo, C. Zhai, D. K. Sun, W. Chen and Q. Li, *J. Mater. Sci. Technol.*, 2019, **9**(35), 309–314.
10 G. E. Marcelle and H. Michael, *J. Alloys Compd.*, 2001, **321**(2), 267–275.
11 G. X. Lu, T. W. Lai, M. G. He and X. Y. Liu, *Chin. Sci. Bull.*, 2020, **65**(7), 641–648.
12 G. Valerio, M. D. Erika, C. Marta, P. Mauro and B. Marcello, *ACS Appl. Energy Mater.*, 2021, **4**(7), 7327–7337.
13 R. E. Thoma, G. D. Brunton, R. A. Penneman and T. K. Keenan, *Inorg. Chem.*, 1970, **9**(5), 1096–1101.
14 J. Van Der Meer, R. Konings, M. Jacobs and H. Oonk, *J. Nucl. Mater.*, 2004, **335**(3), 345–352.
15 M. Berkani and M. Gaune-Escard, *MATEC Web Conf.*, 2013, **3**, 01033.
16 A. Abbasalizadeh, S. Sridar, Z. Chen, M. Sluiter, Y. Yang, J. Sietsma, S. Seetharaman and K. H. Kumar, *J. Alloys Compd.*, 2018, **753**, 388–394.
17 J. Q. Xue, Z. F. Liu, J. Zhang, C. B. Tang and Q. Bi, *Chin. J. Rare Met.*, 2014, **38**(5), 832–838.
18 C. A. Johnathon, S. P. Juliano, A. Mina, A. Y. Jacob, M. M. Amir, E. J. Kaitlin, M. D. Clara and M. B. Theodore, *J. Chem. Thermodyn.*, 2022, **177**, 106931.
19 X. Y. Ye, Q. Li, D. Wu, X. Huang and Y. Luo, *J. Chin. Ceram. Soc.*, 2015, **43**(1), 1597–1604.
20 S. M. Chen, PhD thesis, Jiangxi University of Science and Technology, 2020.
21 C. L. Wang, *Phase diagrams and its application*, 2008, p. 227–227.
22 Z. Y. Qiao, *Handbook of Rare*, 1992, p. 614.
23 Y. Y. Li, *Physicochemical Constants of Rare Earth*, Department of Metals, Sun Yat-Sen University, 1978, p. 93.
24 I. A. Santos, D. Klimm, S. L. Baldochi and I. M. Ranieri, *J. Cryst. Growth*, 2012, **360**, 172–175.
25 I. H. Jung and M. A. V. Ende, *Metall. Mater. Trans. B*, 2020, **51**(5), 1851–1874.
26 S. Li, G. H. Ding, S. H. Wei and Z. M. Cao, *ICPCM, Web of Conferences*, 2014.
27 H. K. Hardy, *Acta Metall.*, 1953, **1**(2), 202–209.
28 M. Schick, A. Watson and K. Hack, *J. Phase Equilib. Diffus.*, 2019, **40**(1), 104–114.
29 S. Renhai, *Thermochim. Acta*, 2020, **683**, 178461.
30 K. H. Kumar and P. Wollants, *J. Alloys Compd.*, 2001, **320**(2), 189–198.
31 O. Redlich and A. T. Kister, *Ind. Eng. Chem.*, 1948, **40**(2), 345–348.